

# Simultaneous two-scale 3D-PTV measurements in turbulence under the influence of system rotation

M. Kinzel · M. Wolf · M. Holzner · B. Lüthi ·  
C. Tropea · W. Kinzelbach

Received: 5 June 2010/Revised: 2 November 2010/Accepted: 8 December 2010/Published online: 31 December 2010  
© Springer-Verlag 2010

**Abstract** We present a technique capable of measuring in a Lagrangian manner the three components of the flow velocity simultaneously at two different spatial resolutions. We use two synchronized 3D Particle Tracking Velocimetry (3D-PTV) systems equipped with filters to separate the two types of seeding particles and measure in volumes of  $55 \times 55 \times 50 \text{ mm}^3$  and  $15 \times 15 \times 15 \text{ mm}^3$ , respectively. In this way, we obtain (a) the velocity field in a large observation volume with focus on the large-scale flow features and (b) velocity derivatives in a small observation volume providing small-scale quantities associated with vorticity and strain. The small observation volume is located in the center of the large one, which allows the small-scale quantities to be related to the large-scale flow patterns. To illustrate the capability of the simultaneous two-scale 3D Particle Tracking Velocimetry (STS 3D-PTV) method, the behavior of vorticity and strain is analyzed in shear-free turbulence under the influence of system rotation. We find that in the quasi-2D region, vortex stretching is strongly suppressed only inside columnar vortex tubes.

## 1 Introduction

When investigating technical and environmental turbulent flows, it is of great interest to measure both large-scale quantities such as overall characteristics of velocity fields and small-scale quantities such as viscous dissipation simultaneously. In order to resolve quantities like the instantaneous dissipation rate, one needs a spatial resolution on the order of the Kolmogorov length scale,  $\eta$ , see, e.g., the PTV experiments by Lüthi et al. (2005), Holzner et al. (2009) or the stereo PIV method in Mullin and Dahm (2009). The numerical results in Schumacher (2007) indicate that a resolution of three to five  $\eta$  reproduces faithfully the flow at scales about two times smaller than those resolved, at least as far as the instantaneous dissipation rate is concerned. Unfortunately, there is a trade-off in all whole field measurement techniques between the achievable spatial resolution and the size of the observation area or volume. In three-dimensional Particle Tracking Velocimetry (3D-PTV), for example, the number of particles which can be tracked is determined by the resolution of the cameras. The main limiting parameter is the spatial resolution of the cameras, which determines the maximum seeding density for which particle positions can still be detected and stereo-matched reliably. With a common camera resolution of  $1,000 \times 1,000$  pixels and a four camera PTV setup, it is possible to track at most a few thousand particles simultaneously. In addition, the temporal resolution of the cameras has to be adequate, since it determines the ability of the system to reliably track the motion of tracer particles over time. The so-called ‘tracking parameter’, e.g., Dracos (1996), which is defined as the ratio between the average particle displacement between two frames and the average interparticle distance should be smaller than one to guarantee good trackability. Since the maximum number of

---

M. Kinzel (✉) · M. Wolf · C. Tropea  
Institute of Fluid Mechanics and Aerodynamics (SLA),  
Technische Universität Darmstadt, Darmstadt, Germany  
e-mail: m.kinzel@sla.tu-darmstadt.de; m.kinzel@gmx.net

M. Wolf · M. Holzner · B. Lüthi · W. Kinzelbach  
Institute of Environmental Engineering (IfU),  
Swiss Federal Institute of Technology, Zurich, Switzerland

C. Tropea  
Center of Smart Interfaces (CSI),  
Technische Universität Darmstadt, Darmstadt, Germany

particles is fixed by the camera resolution, the only possibility to increase the spatial resolution is to decrease the size of the observation volume. Other whole field methods have similar limitations.

A spatial resolution of 0.005 particles per pixel (ppp), which is common for PTV, is also achievable with Holographic Particle Image Velocimetry (HPIV) and Defocussing Particle Image Velocimetry (DPIV), see Barnhart et al. (1994) and Pereira et al. (2000). The possible seeding density of Tomographic Particle Image Velocimetry (Tomo-PIV) is an order of magnitude higher than in 3D-PTV ( $\approx 0.05$  ppp), see Elsinga et al. (2006). But the connection between the observation volume size and the spatial resolution is the same, i.e., for larger fields of view the spatial resolution decreases. In order to achieve higher spatial resolution, scanning techniques have been applied in PIV and PTV measurements, see Brücker (1995) and Hoyer et al. (2005). The idea is to divide a large observation volume into smaller slices and consecutively record these slices with a scanning rate, which is high compared to the time scales of the flow. The drawback is a loss in temporal resolution.

In principle, it is possible in steady-state flows to perform two consecutive measurements with two different observation volume sizes and spatial resolutions to capture both the large and small spatial scales. However, the majority of flows observed in engineering applications and nature are turbulent, i.e., time dependent and statistically steady state at best. In turbulence, eddy sizes range from the largest size, the integral scale  $\ell$ , down to the dissipative scale, the Kolmogorov length scale  $\eta$ . The Reynolds number of the flow determines the separation between the largest and smallest sizes, according to  $\ell/\eta \propto \text{Re}^{3/4}$ , Tennekes and Lumley (1972). In order to understand the coupling between different ranges of scales, all relevant quantities must be measured simultaneously.

The method we propose here is to follow the approach of Guala et al. (2008) who performed measurements in a two-phase flow using two different PTV systems simultaneously, where one system was used to follow tracers in the liquid phase and the second system to track suspended sediment particles. This approach is extended herein to perform simultaneous measurements at different spatial resolutions using two synchronized PTV systems. Namely, we measure (a) the velocity in a large observation volume with focus on the large-scale flow features and (b) velocity derivatives in a small observation volume, which provide small-scale quantities associated with vorticity and strain. The small observation volume is located in the center of the large one, which allows the small-scale quantities to be related to the large-scale flow pattern.

The flow which we investigate and which serves to demonstrate the potential of the Simultaneous two-scale 3D-PTV method (STS 3D-PTV) is shear-free turbulence under the influence of system rotation. A well-known, yet not completely understood, macroscopic effect of system rotation on turbulence is the appearance of large columnar structures (e.g., Hopfinger et al. (1982)). Extensive research, both experimental (e.g., Hopfinger et al. (1982), Morize et al. (2005), Davidson et al. (2006), Kinzel et al. (2009a, b)) and numerical (e.g., Godefert and Lollini (1998), Mininni et al. (2009)), has been performed with focus on these structures, which are commonly associated with a qualitative change of the flow from a three-dimensional to a more two-dimensional state. With increasing Taylor microscale Reynolds number,  $\text{Re}_\lambda$ , and rotational velocity,  $\Omega$ , the number of columnar structures is known to increase, while their diameter decreases. Their formation has been associated with inertial waves, see, e.g., Hopfinger et al. (1982) and Davidson et al. (2006). The influence, which system rotation has on turbulent flows is expected to have strong effects both at the large- and at small-scale level, also due to the strong coupling between the two. With the suppression of self-amplification of the strain and vorticity field, the anisotropy (i.e., two dimensionalization) at the large-scale level is presumably associated with the 'disappearance' of the turbulent small-scale structure with decreasing Rossby number (Tsinober 2009). This has been observed qualitatively, e.g., by using streakline photographs in McEwan (1976), see also Tsinober (2009). To the best of our knowledge, up to now, there are no measurements of the 3D small-scale structure of turbulence under the influence of system rotation in the literature. One of the reasons is the above-mentioned difficulty of resolving the full range of eddy sizes simultaneously. Our aim is to provide experimental information on the behavior of the small-scales quantities in the regions, which are classified according to the large-scale flow pattern (e.g., vortex core or regions in between columnar vortices). To achieve this, the large observation volume was used to detect the columnar vortex structures while the full velocity gradient tensor is accessed in the small volume at the same time.

The next section describes the experimental rig, the details of the STS 3D-PTV system and the method, which is applied to identify the vortex columns. In Sect. 2, the accuracy of the measured particle positions, velocities and accelerations is compared for the large and small observation volume. The results, which characterize the vortex columns and demonstrate the advantages of the STS 3D-PTV method, are presented in Sect. 3 Finally, conclusions are drawn and a summary given in Sect. 4.

## 2 Method

### 2.1 Experimental rig

The measurements have been carried out in a  $200 \times 200 \times 300 \text{ mm}^3$  water tank in which the flow is mechanically forced from the top by an oscillating grid, see Fig. 1. The grid has a cross-type fractal pattern, with a maximum bar width of 4 mm and three fractal iterations (see Hurst and Vassilicos (2007) for details). The advantage of the fractal grid is that it injects more energy into the flow and forces a wider range of scales (see Hurst and Vassilicos (2007)). Therefore, the minimal distance at which the turbulence can be considered homogeneous in planes parallel to the grid is reduced, and higher turbulence intensities can be achieved than with classical grids which have a similar blockage ratio.

In the experimental setup, the grid is connected to a linear motor, which drives the vertical oscillation on a supporting frame connected to the grid by four rods, each 4 mm in diameter, Fig. 1. The motor, operated in a closed loop with feedback from a linear encoder, was set at a frequency of 9 Hz and an amplitude of  $\pm 4 \text{ mm}$  for all the experiments (see Holzner et al. (2006) for more details). Relevant flow parameters were estimated in an experiment without system rotation. The measured r.m.s. velocity of the flow was about 10 mm/s and we estimated the Kolmogorov length scale to be  $\eta = 0.4 \text{ mm}$  using the expression  $\eta = (v^3/\epsilon)^{1/4}$ , where the dissipation is given by  $\epsilon = 2\nu\langle s_{ij}s_{ij} \rangle$ , the angle brackets denoting an average over space and time, and  $s_{ij}$  are the components of the rate of strain tensor directly measured via 3D-PTV. The Taylor microscale,  $\lambda$ , was about 6 mm, and the Kolmogorov time scale,  $\tau_\eta$ , was estimated as 0.3 s. The Taylor microscale Reynolds number is  $\text{Re}_\lambda = 60$ .

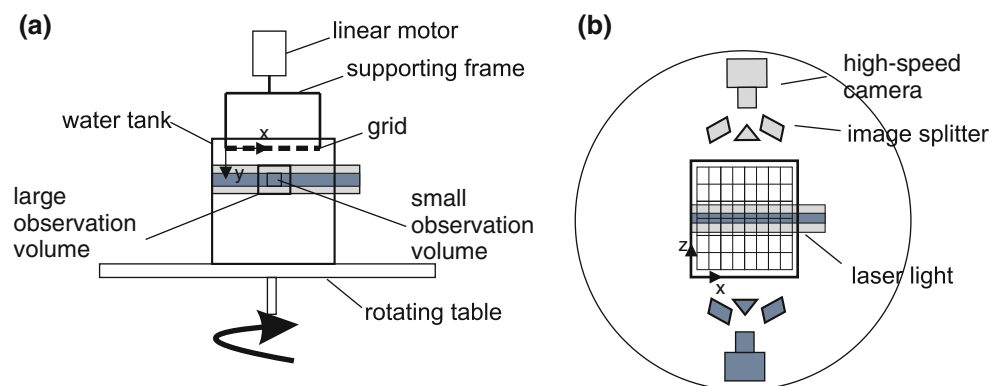
Also, the entire setup was placed on a rotating table with a diameter of 1 m, allowing for rotation rates up to 3.14 rad/s (see Fig. 1). The power supply and the control of the grid are provided through a slip ring at the base of the rotating table.

It is well known that in oscillating grid chambers, some weak mean flow can arise, see, e.g., Orlns and Gulliver (2003). In the experiments without system rotation, baffles were installed at the bottom of the tank to keep this mean flow to a minimum. The weak mean flow which remains is subtracted from the data, i.e., the results focus on the fluctuating velocity field only. In the experiments under the influence of system rotation, the rotational forces inhibit the formation of three-dimensional recirculation cells.

### 2.2 STS 3D-PTV

Following the work of Kinzel et al. (2009), who performed 3D-PTV measurements in a small and a large observation volume successively in the present study, 3D-PTV measurements were performed simultaneously with two different spatial resolutions. Two PTV systems were set up on opposite sides of the tank. Both systems use image splitters, one is mounted in front of a Photron APX and the other in front of a Photron Fastcam high-speed camera (both  $1,024 \times 1,024 \text{ pixels}^2$ ). Each image splitter consists of four mirrors, which are arranged around a mirror pyramid and mimic a four camera setup (see Hoyer et al. (2005)). Both cameras were triggered by the same signal and their frame rate was 125 Hz though the camera for the small observation volume was operated at a shutter speed of 5 ms. A CAD drawing shows how the two systems are arranged on the rotating table, see Fig. 2. A key element of the simultaneous two-scale measurements is the seeding, which has to be different for the two observation volumes. Polystyrene particles with a diameter of  $60 \mu\text{m}$  were employed for the large observation volume and fluorescent particles with a diameter of  $80 \mu\text{m}$  for the small observation volume. It was necessary to use a larger particle diameter in the small volume because of the significantly lower light intensity emitted through fluorescence when compared to Mie scattering. Both cameras were equipped with dichroic color filters (green/550 nm for the Polystyrene and red/590 nm for the Polystyrene Rhodamin B particles) to

**Fig. 1** Schematic of the experimental setup with the position of the two observation volumes for the STS 3D-PTV measurements as seen from the front (a) and top (b)



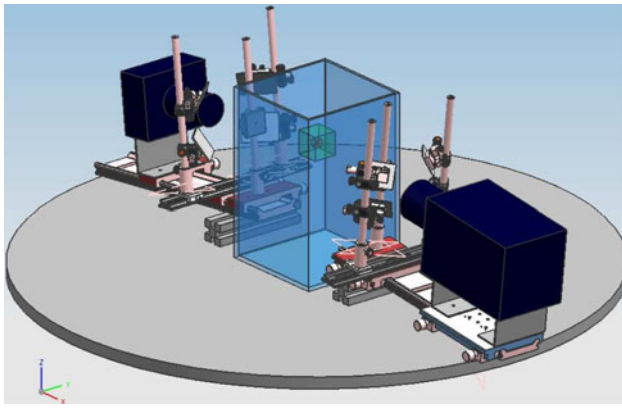


**Fig. 2** CAD sketch of the two PTV systems including the large and the small observation volume

separate the two types of seeding particles. Additionally, the illumination of the observation volumes has to be adapted since the light intensity needed for the illumination of the small observation volume is considerably higher than for the large observation volume and the available laser light was not sufficient to illuminate the large volume in the intensity needed for the small volume. Furthermore, a full opening of the aperture is not possible as this would reduce the depth of focus too much. Since only one laser was available, the laser beam was expanded through spherical lenses to illuminate a small observation volume of size  $15 \times 15 \times 15 \text{ mm}^3$ . After passing through the tank, the beam is reflected, expanded further to the size of the large observation volume ( $55 \times 55 \times 50 \text{ mm}^3$ ) and sent back through the tank. The observation volumes are located at the upper end of the tank underneath the lowest grid position, see Figs. 1 and 2. It was possible to achieve interparticle distances of  $9.5\eta$  and  $2.5\eta$  in the large and the small observation volumes, respectively. The measurement accuracy of the particle positions was determined during the calibration where the known particle positions of the calibration target are compared to the positions reconstructed from the calibration images by the PTV algorithm. These accuracies were found to be approximately 0.035 mm in x- and y- and 0.09 mm in z-direction for the large observation volume and 0.02 mm and 0.045 mm for the small observation volume. Also, for these experiments, the Stokes numbers of the two kinds of seeding particles were calculated to be on the order of  $10^{-3}$  based on the Kolmogorov time scale,  $\tau_n = (\nu/\epsilon)^{1/2}$ , assuring that the particles follow the flow reliably. Furthermore, the particle and fluid densities were carefully matched to a density of  $1.05 \text{ g/cm}^3$  using salt.

Guala et al. (2008) used a similar configuration to perform simultaneous measurements of the fluid and the solid phase in a two-phase PTV experiment. They constructed a

planar calibration target for a multi-plane cross-calibration of two PTV observation volumes. The target consists of two identical aluminum plates with conical holes and aluminum foil with a thickness of less than  $10 \mu\text{m}$  between them. In this work, the same device is used to focus both camera systems on the same x–y plane in the center of the observation volumes. Each PTV system was then calibrated with a separate three-dimensional calibration target, namely the ones used by Lüthi (2002). Both targets were positioned with a 3D-traversing system inside the tank. The offset between them is thus known, and the data from the small observation volume can be easily transformed to the coordinate system of the large observation volume. The checks in the following section show that this procedure yields accuracies for the particle positions and velocities as though both measurements are carried out separately.

### 2.3 Checks

Velocity derivatives were obtained from the measurements using the method introduced by Lüthi et al. (2005), which involves two steps: a local linear interpolation of the velocity field and a weighted polynomial fit to the derivatives along particle trajectories. Velocity derivatives with a low spatial resolution were obtained from the experiment in the large observation volume, while velocity derivatives with high spatial resolution are available from the data measured in the small observation volume. First, following the approach of Lüthi et al. (2005), statistical checks based on precise kinematic relations were performed to validate our methodology and to assess the accuracy of the measurements of velocity gradients for both 3D-PTV systems individually. This was previously accomplished in Kinzel et al. (2009a) for the case in which both volumes were measured separately and the results of the simultaneous measurements look practically the same.

The cross-calibration of the two PTV systems can be validated by using particle trajectories measured with both systems, see Guala et al. (2008). For this, an experiment was performed in which the color filters were removed from the cameras so that both PTV systems record the images of the same seeding particles, allowing a pointwise comparison of the results obtained from both systems. From this experiment, the pointwise differences in the measured particle positions, velocities and accelerations were calculated. Figure 3 illustrates an example of a particle trajectory, which was tracked simultaneously with both PTV systems. The trajectory measured in the large (red) and the small (blue) observation volume almost overlap. On the order of  $5 \times 10^5$ , data points, which were obtained simultaneously with both systems, were used to calculate PDFs of the

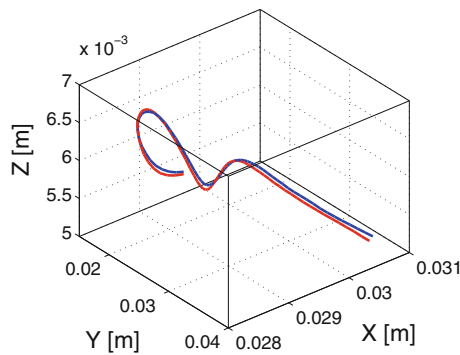


**Fig. 3** Particle trajectory as recorded simultaneously in the large (red) and the small (blue) observation volume

differences in the particle positions, velocities and accelerations, see Fig. 4a, b and c, respectively.

The r.m.s. of the difference between the particle locations obtained with the two systems,  $\Delta x$ , is of the order of  $100 \mu\text{m}$ , which is slightly larger than the diameter of the seeding particles or the accuracy in the position measurements. The mean value of  $\Delta x$  is below  $11 \mu\text{m}$ . The differences in the measured velocities and accelerations are of the order of  $10^{-3} \text{ m/s}$  and  $10^{-1} \text{ m/s}^2$ , respectively, which is better than the accuracy associated with the respective quantity (see Lüthi et al. (2005)). Since the mean is non-zero, there is a small bias in the PDFs of  $\Delta v$  and  $\Delta w$ .

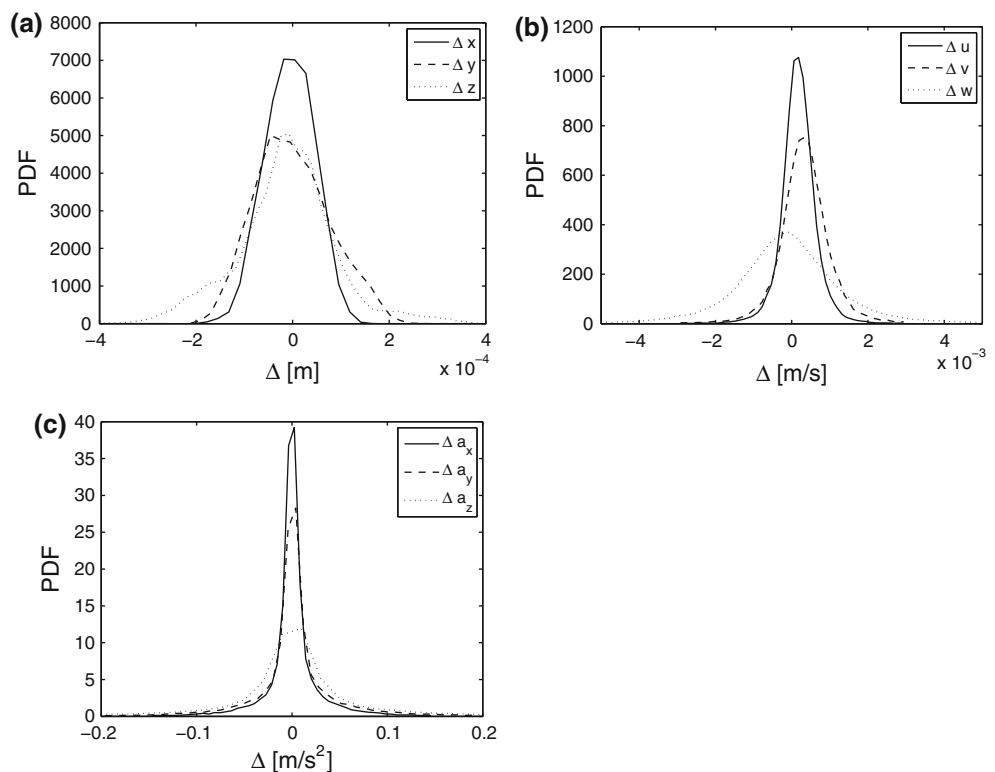
However, these biases are an order of magnitude smaller than the measured velocities and therefore tolerable.

### 2.4 Detection of the columnar vortices

As mentioned above, one of the striking large-scale characteristics of turbulence in a rotating system is the occurrence of columnar vortices approximately aligned with the axis of rotation. This section describes how the method introduced by Michard et al. (1997) to detect vortices in 2-D velocity fields is applied to detect vortex columns in the observation volume.

The influence of system rotation on the turbulent flow is quantified by the Rossby number,  $\text{Ro} = U/2\Omega L$ , where  $U$  and  $L$  are the local characteristic fluctuating velocity and integral length scale of the turbulent flow, and  $\Omega$  is the external angular velocity.  $\text{Ro}$  is the ratio between advective acceleration,  $u \cdot \nabla u \propto U^2/L$ , and rotational acceleration,  $\Omega \times u \propto U\Omega$ , i.e., large  $\text{Ro}$  corresponds to a dominance of the advection term; hence, a negligible influence of rotation, and small  $\text{Ro}$  corresponds to a strong influence of the rotational term. In the proximity of the grid, the advective term dominates, which is reflected in a large local  $\text{Ro}$  and an insignificant influence of the rotational forces. With increasing distance from the grid, the velocity decreases with  $u \propto y^{-1}$  and thus the advective term behaves proportionally to  $u\partial u/\partial x \propto y^{-2}$ , see Holzner et al. (2008). The

**Fig. 4** PDFs of the difference in position (a), velocity (b) and acceleration (c) measurements between the large and the small observation volume



rotational forces, which depend on the flow velocities, decrease as  $u \propto y^{-1}$ , see, e.g., Silva and Fernando (1994). This causes a dominance of the rotational term and a small Ro. The consequence is a quasi-2D flow, which evolves below a distance  $y^*$  from the grid, where the rotational accelerations outweigh the advective ones. In agreement with, e.g., Hopfinger et al. (1982), this quasi-2D region was observed to evolve at a local Rossby number of approximately 0.2 (see also Lüthi et al. (2008)). As observed in Kinzel (2010) (see also, e.g., Hopfinger et al. (1982), Godefert and Lollini (1998)), this flow region is strongly dominated by columnar vortex structures which we identify based on the method introduced by Michard et al. (1997). The method calculates the mean angular momentum,  $\Gamma_1$ , of the horizontal velocity components  $u$  and  $w$  measured at the particle locations  $M$  around the arbitrary point  $P$  (compare Eq. 1 and Fig. 5a).

$$\Gamma_1 = \frac{1}{N} \sum_s \frac{(\mathbf{PM} \times \mathbf{u}_M) \cdot \mathbf{e}_z}{\|\mathbf{PM}\| \cdot \|\mathbf{u}_M\|}, \quad (1)$$

where  $s$  is the measurement domain and  $\mathbf{e}_z$  the unit vector perpendicular to the 2D-velocity field. According to Michard et al. (1997), the point  $P$  is located in the center of a vortex column if  $0.9 < |\Gamma_1| < 1$ . We calculate  $\Gamma_1$  on a regular grid of points  $P$  throughout the large observation volume, and the resulting field can be observed in Fig. 5b. The size of the cylindrical data slice around each point  $P$  from which  $\Gamma_1$  is calculated is chosen to be of the same size as the diameter of the columnar vortices, i.e., 50 mm. Thus, the  $\Gamma_1$  distribution of a given vortex only depends on the vortex itself and its immediate surrounding.

### 3 Results

To illustrate the necessity of the small measurement volume with the higher spatial resolution, the behavior of

the second and third invariants of the velocity gradient tensor is analyzed. While the second invariant expresses to the relative strength of enstrophy and strain,  $Q = 1/4(\omega^2 - 2s^2)$ , the third compares their production terms,  $R = -1/3(s_{ij}s_{jk}s_{ki} + 3/4\omega_i\omega_j s_{ij})$ . In homogeneous, statistically stationary turbulence, the iso-probability contours in the R-Q joint PDF are known to have a characteristic ‘tear-drop’ shape with a distinct region in the second quadrant representing the swirling motion of turbulence ( $Q > 0, R < 0$ ) and the ‘Vieillefosse Tail’, (Vieillefosse 1982) in the fourth quadrant representing the strong dissipative events that occur in turbulence ( $Q < 0, R > 0$ ). An example of this shape can be seen in Fig. 6a, where the data recorded in the small observation volume are presented from a turbulent flow without system rotation. Figure 6b on the other hand depicts the same experimental data but recorded in the large observation volume. While the iso-contours from the small observation volume yield the tear-drop shape (Fig. 6a), the results obtained from the lower resolved data fail to capture the ‘Vieillefosse Tail’ and mainly follow a Gaussian behavior (Fig. 6b), see also Lüthi et al. (2007).

The usefulness of the STS 3D-PTV method becomes apparent when analyzing the data from a simultaneous recording at a rotation rate of 3.14 rad/s. The qualitatively different regions of the flow (i.e., the vortex core and the region between the vortex columns) are identified based on the information from the large observation volume and coupled with the small-scale information from the high resolution measurement. As an example, the behavior of the vortex stretching vector,  $W_i \equiv \omega_j \frac{\partial u_i}{\partial x_j} = \omega_j s_{ij}$ , which represents the interaction between vorticity and the rate of strain tensor, is discussed. An alignment between the vorticity and the vortex stretching vectors implies vortex stretching, while negative alignment between the two vectors corresponds to vortex compression.

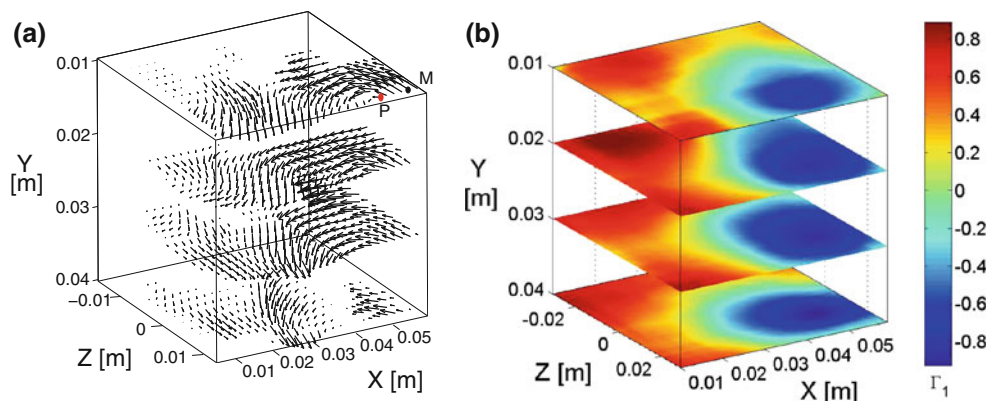
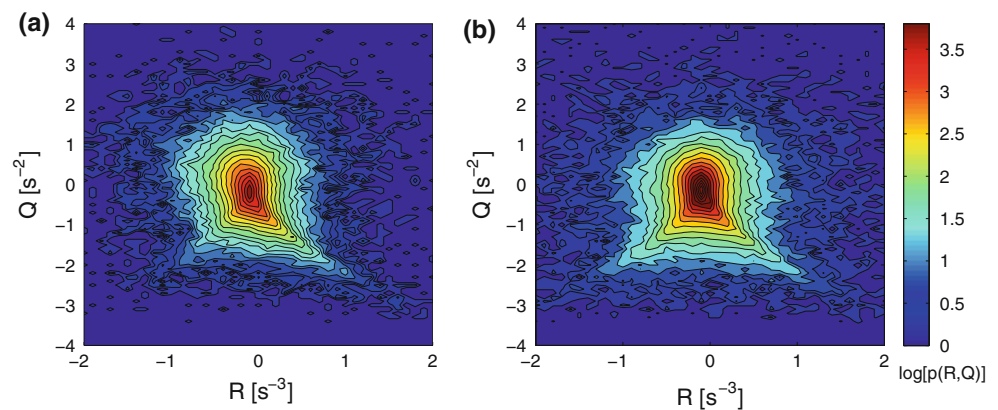


**Fig. 5** Instantaneous velocity vector field with a schematic of the points  $P$  and  $M$  (a) and corresponding contour maps of  $\Gamma_1$  (b) from an experiment with a rotational velocity of 3.14 rad/s

**Fig. 6** Joint PDF of R versus Q for the small (a) and the large observation volume (b)



The PDFs of the cosine of the angle between the vorticity and the vortex stretching vectors,  $\cos(\omega, W)$ , are presented in Fig. 7a for the region of the vortex columns (dotted,  $|\Gamma_1| > 0.3$ ), the region in between the columnar structures (dashed,  $|\Gamma_1| < 0.3$ ), and in the non-rotating turbulent flow (solid). For the latter, the PDF is skewed toward one, which reflects the dominance of vortex stretching for three-dimensional turbulence (Tsinobir (2009)). For the case with system rotation, we note that the positive skewness of the PDFs is reduced in favor of a higher probability of negative events (vortex compression). This effect is more pronounced for the vortex cores than for the region in between vortex columns (Fig. 7a).

The conditional average of the cosine of the angle between vorticity and the vortex stretching vectors,  $\langle \cos(\omega, W) \rangle$ , over  $\Gamma_1$  is presented in Fig. 7b. The data allow to calculate the conditional average for magnitudes of  $\Gamma_1$  smaller than 0.7.  $\langle \cos(\omega, W) \rangle$  is negative in the core region of the vortex columns, which suggests a dominance of vortex compression. With distance from the core of the vortex columns,  $\langle \cos(\omega, W) \rangle$  increases continuously until it reaches a plateau between  $-0.3 < \Gamma_1 < 0.3$ . This plateau close to 0.08 corresponds to the region in between the

vortex columns and is close to the value of 0.1 known for turbulence without system rotation.

#### 4 Conclusions

Simultaneous two-scale 3D-PTV measurements have been performed in a turbulent flow under the influence of system rotation. With interparticle distances of  $9.5\eta$  in a large observation volume and  $2.5\eta$  in a small volume, it was possible to capture the large-scale flow pattern and to simultaneously measure small-scale quantities like vorticity and strain. The accuracies in the measured derivatives of the velocity tensor were similar to the results in Kinzel et al. (2009a) for the experiments, in which measurements were carried out in both observation volumes consecutively. The spatial difference between the particle locations measured in the two volumes was found to be on the order of  $100\ \mu\text{m}$ , which is slightly larger than the diameter of the seeding particles. The differences in the measured velocities and accelerations are of the order of  $10^{-3}\ \text{m/s}$  and  $10^{-1}\ \text{m/s}^2$ , respectively, which is smaller than the measurement accuracy of these quantities.

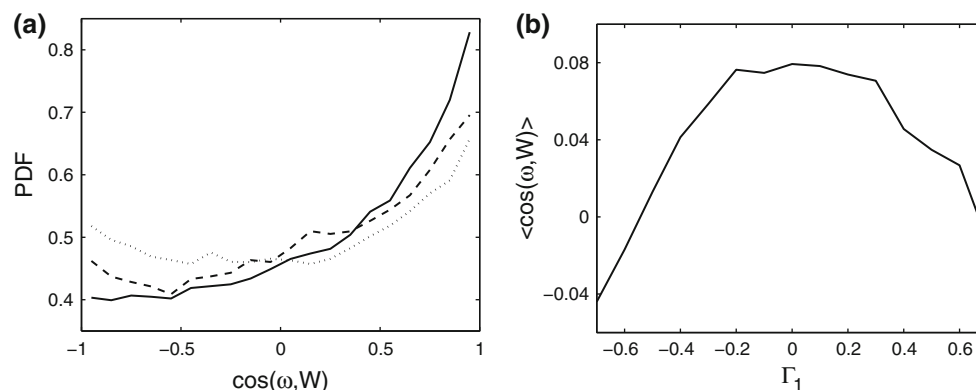


**Fig. 7** PDFs for the region of the vortex columns (dotted), the region in between the columnar structures (dashed) and for an experiment without system rotation (solid) (a) and cosine of the angle between  $\omega$  and  $W$  conditionally averaged over  $\Gamma_1$  (b)

The large observation volume was used to detect the columnar structures based on the angular momentum method introduced by Michard et al. (1997). This allowed to condition the data on different flow regions, i.e., inside and in between the vortex columns. The difference between the two regions on the level of small scales was illustrated at the behavior of the vortex stretching vector. It could be shown that system rotation reduces the vortex stretching mechanism characteristic for 3D-turbulence and enhances vortex compression. This occurs strongest in the region of the vortex columns, while the flow in between the columnar structures exhibits a behavior closer to that of the 3D turbulent flow on the level of vortex stretching. Together, this demonstrates the usefulness of the simultaneous two-scale measurements.

In the present work, the scale separation is rather small ( $Re_\lambda \approx 60$ ). However, the potential of the method is clear. The next step is to apply the STS 3D-PTV method to higher Reynolds number flows.

**Acknowledgments** The financial support by the German Research Foundation (DFG) under grant Tr. 194/37-4 is gratefully acknowledged. Furthermore, the authors would like to thank A. Tsinober for his contributions to this work.

## References

- Barnhart D, Adrian R, Papen G (1994) Phase-conjugate holographic system for high-resolution Particle-Image Velocimetry. *Appl Opt* 33:7159–7170
- Brücker C (1995) Digital-Particle-Image-Velocimetry (DPIV) in a scanning light-sheet: 3D starting flow around a short cylinder. *Exp Fluids* 19:255–263
- Davidson PA, Staplehurst PJ, Dalziel S (2006) On the evolution of eddies in a rapidly rotating system. *J Fluid Mech* 557:135–144
- Dracos, T (eds) (1996) Three-dimensional velocity and vorticity measuring and image analysis techniques. Kluwer, Dordrecht
- Elsinga G, Scarano F, Wieneke B, Oudheusden BV (2006) Tomographic particle image velocimetry. *Exp Fluids* 41:933–947
- Godefert F, Lollini L (1998) Direct numerical simulations of turbulence with confinement and rotation. *J Fluid Mech* 393:257–308
- Guala M, Liberzon A, Hoyer K, Tsinober A, Kinzelbach W (2008) Experimental study of clustering of large particles in homogeneous turbulent flow. *J Turbulence* 9(34):1–20
- Holzner M, Liberzon A, Guala A, Tsinober A, Kinzelbach W (2006) Generalized detection of a turbulent front generated by an oscillation grid. *Exp Fluids* 41(5):711–719
- Holzner M, Liberzon A, Nikitin N, Lüthi B, Kinzelbach W, Tsinober A (2008) A lagrangian investigation of the small scale features of turbulent entrainment through 3D-PTV and DNS. *J Fluid Mech* 598:465–475
- Holzner M, Lüthi B, Kinzelbach W, Tsinober A (2009) Acceleration, pressure and related quantities in the proximity of the turbulent/nonturbulent interface. *J Fluid Mech* 639:153–165
- Hopfinger EJ, Browand FK, Gagne Y (1982) Turbulence and waves in a rotating tank. *J Fluid Mech* 125:505–534
- Hoyer K, Holzner M, Lüthi B, Guala M, Liberzon A, Kinzelbach W (2005) 3D scanning particle tracking. *Exp Fluids* 39(7):923–934
- Hurst D, Vassilicos J (2007) Scaling and decay of fractal-generated turbulence. *Phys Fluids* 19:035103
- Kinzel M (2010) Experimental investigation of turbulence under the influence of confinement and rotation. PhD Thesis
- Kinzel M, Holzner M, Lüthi B, Liberzon A, Tropea C, Kinzelbach W, Oberlack M (2009) Two-scale experiments via Particle Tracking Velocimetry: a feasibility study. *Imaging Measurement Methods, Notes on Numerical Fluid Mechanics and Multidisciplinary Design* 106:103–111
- Kinzel M, Holzner M, Lüthi B, Tropea C, Kinzelbach W, Oberlack M (2009) Experiments of the spreading of shear-free turbulence under the influence of confinement and rotation. *Exp Fluids* 47:801–814
- Lüthi B (2002) Some aspects of strain, vorticity and material element dynamics as measured with 3D Particle Tracking Velocimetry in a turbulent flow. PhD Thesis
- Lüthi B, Tsinober A, Kinzelbach W (2005) Lagrangian measurement of vorticity dynamics in turbulent flow. *J Fluid Mech* 528:87–118
- Lüthi B, Ott S, Berg J, Mann J (2007) Lagrangian multi-particle statistics. *J Turbulence* 8:1468–5248
- Lüthi B, Kinzel M, Liberzon A, Holzner M, Tropea C, Kinzelbach W, Tsinober A (2008) 3d-2d transition in inhomogeneous rotating turbulent flow. *ERCOFTAC Special Bulletin on Environmental Flows*
- McEwan A (1976) Angular-momentum diffusion and initiation of cyclones. *Nat Biotechnol* 260(5547):126–128
- Michard M, Graftieaux L, Lollini L, Grosjean N (1997) Identification of vortical structures by a non-local criterion: Applications to P.I.V. measurements and D.N.S results of turbulent rotating flows. In: *Proceedings of Eleventh Symposium on Turbulent Shear Flows, Grenoble*
- Mininni PD, Alexakis A, Pouquet A (2009) Scale interactions and scaling laws in rotating flows at moderate Rossby numbers and large Reynolds numbers. *Phys Fluids* 21:015,108
- Morize C, Moisy F, Rabaud M (2005) Decaying grid-generated turbulence in a rotating tank. *Phys Fluids* 17:095,105
- Mullin J, Dahm W (2009) Dual-plane stereo particle image velocimetry measurements of velocity gradient tensor fields in turbulent shear flow. *Phys Fluids* 18:035,101
- Orlins J, Gulliver J (2003) Turbulence quantification and sediment resuspension in an oscillating grid chamber. *Exp Fluids* 34:662–677
- Pereira F, Gharib M, Dabiri D, Modarress M (2000) Defocusing DPIV: a 3-component 3-D DPIV measurement technique. application to bubbly flows. *Exp Fluids* 29:78–84
- Schumacher J (2007) Sub-Kolmogorov-scale fluctuations in fluid turbulence. *Europhys Lett* 80. arXiv:0710.4100v1
- Silva ID, Fernando H (1994) Oscillating grids as a source of nearly isotropic turbulence. *Phys Fluids A* 6(7):2455–2464
- Tennekes H, Lumley J (1972) *A first course in turbulence*. MIT Press, Cambridge
- Tsinober A (2009) *An informal conceptual introduction to turbulence*. Springer, Berlin
- Vieillefosse P (1982) Local interaction between vorticity and shear in a perfect incompressible fluid. *Le J de Physique* 43:837–842